Chapter 2

Oscillations in a Magnetized Atmosphere [1]

In this chapter we will show that even in the presence of a weak vertical magnetic field the acoustic modes, which are a main focus of the remainder of this dissertation, still exist, though they are mildly altered by the magnetic field. This, in a sense, justifies treating magnetic field as a small perturbation when discussing the helioseismology of the quiet Sun. The main effect of the weak magnetic field, we will see, is to introduce new magnetic modes: Alfvén modes for small horizontal wavenumber and slow modes modified by gravity at high wavenumber. The magnetic field also introduces instabilities, in particular in the neighborhood of avoided crossings. This is potentially important for dynamical phenomena such as spicules. The precise role, however, of these instabilities is not yet clear as we are working with a simple model. A full understanding of these instabilities will require numerical simulations and is beyond the scope of this dissertation.

[1] *This chapter is mostly from the Solar Physics article by Birch, Kosovichev, Spiegel, & Tao (2001b). I wrote sections 2.3, 2.4, and 2.5. The remaining sections were written by E. Spiegel and L. Tao and I have performed only minor editing on the original text. I carried out the analytical and numerical work for the paper, with the exception of the work for the first figure, which was done by L. Tao.*

Abstract

We perform linear stability analysis on stratified, plane-parallel atmospheres in uniform vertical magnetic fields. We assume infinite electrical conductivity and we model non-adiabatic effects with Newton's law of radiative cooling. Because of these numerous simplifying assumptions we expect the results of this analysis to be qualitative at best. Numerical computations of the dispersion diagrams in all cases result in patterns of avoided crossings and mergers in the real part of the frequency. We focus on the case of a polytrope with a prevalent, relatively weak, magnetic field with overstable modes. The growth rates reveal prominent features near avoided crossings in the diagnostic diagram, as has been seen in related problems (Banerjee *et al.*, 1997). These features arise in the presence of resonant oscillatory bifurcations in non-self adjoint eigenvalue problems. The onset of such bifurcations is signaled by the appearance of avoided crossings and mode mergers. We discuss the possible role of the linear stability results in understanding solar spicules.

2.1 Introduction

There is no shortage of instabilities that may provoke solar activity, and more are being discovered. The problem is rather to anticipate how the situation will change as these instabilities develop. Surprisingly, a lot of the nonlinear development of an instability can be foretold on the basis of its linear theory with the help of the normal form theory (Guckenheimer & Holmes, 1983). This theory provides generic forms of the nonlinear equations for the amplitudes of unstable modes for given instability configurations. Though it is a rather formal theory, it is an informative one that has provided some guidance in some circumstances, such as stellar pulsation theory (Regev & Buchler, 1981; Spiegel, 1993). However, there are cases that are only now being unraveled and these relate to situations called resonant Hopf bifurcations where negative energy modes may occur. These modes can promote rapid growth and vigorous activity and their presence is usually signaled by the avoided crossings of modes.

Avoided crossings, or avoided level crossings, are known in quantum mechanics, where their behavior is related to the onset of chaos in the corresponding classical system, and are widely found in fluid instabilities, stellar instabilities being no exception. Here we join the chorus of analysts of such interesting linear problems with a brief discussion of avoided crossings in the context of nonadiabatic magnetoacoustic instability of a stratified atmosphere. But before presenting some dispersion relations for this problem, we would like to make some elementary remarks to set the stage for the discussion.

2.2 The Resonant Hopf Bifurcation

To review briefly the nature of level crossings, we consider small perturbations to a plane-parallel equilibrium model. This generally gives rise to a dispersion relation $\mathcal{D}(\Omega, k, n) = 0$ where Ω is the time constant of the mode – the real part of Ω is the frequency — k is its horizontal wavenumber and n is the vertical mode label.

Where two roots of the dispersion relation nearly coincide, the dispersion relation can be approximated by an equation of the form (e.g. Lee & Saio, 1989):

$$[(\omega - \omega_0) - u(k - k_0)]\,[(\omega - \omega_0) - v(k - k_0)] - \epsilon = 0\,. \tag{2.1}$$

Here u and v are the slopes of the asymptotes in the $k - \omega$ diagram, so that the dispersion relations are $\omega = \omega_0 + u(k - k_0)$ and $\omega = \omega_0 + v(k - k_0)$ away from the crossing. The parameter ϵ represents the coupling between the two modes at resonance.

In the presence of radiative cooling or other forms of damping, taking the simplest case that the damping is independent of wavenumber at resonance, we may assume that the dispersion relation takes the following form:

$$[(\omega - \omega_0 + \alpha i) - u(k - k_0)]\,[(\omega - \omega_0 + \beta i) - v(k - k_0)] - \epsilon = 0 \tag{2.2}$$

where α and β are the damping rates, and the coupling ϵ may be complex. In the simple situation we shall treat, we assume that *locally* the damping rate is independent of the horizontal wavenumber k so that the parameters α and β do not depend on k. We shall see later that the resulting dispersion relations qualitatively describe our physical system.

In Figure 2.1 we plot three representative solutions. In the top panel, we see that the frequencies exhibit an avoided crossing, but the imaginary parts do cross. The size of the gap at avoided crossings is directly proportional to the coupling, ϵ. In the middle panel, the behavior of the real and imaginary parts is contrary to that in the top panel: the avoidance is seen in the imaginary part, while the real parts of the frequency cross. In the bottom panel, we see a merger of the real parts, accompanied with a splitting of the imaginary parts. In this symmetric situation, the roots are exactly complex conjugates when the branches merge. Under very general conditions, two otherwise stable modes interact resonantly to produce one unstable mode.

In the astrophysical context, avoided crossings of the kind illustrated here are familiar in non-radial stellar oscillations (Aizenman et al., 1977; Lee & Saio, 1990) and our particular interest here is in their effects on growth rates of magnetoacoustic instabilities, to which we now turn.

2.3 Equations and Equilibria

Linearized perturbations about model equilibrium atmospheres and their dynamics may be described by the ideal magnetohydrodynamics (MHD) equations. Here we assume that the gas is governed by the ideal gas law and is nonadiabatic.

Let ρ, P, and $\mathbf{v}$ denote the density, pressure, and velocity of the gas and $\mathbf{B}$ and $\mathbf{J}$ denote the magnetic field strength and the current. The speed of light is c_l. Then the set of ideal MHD equations consists of the continuity equation, the momentum equation, the heat equation for the gas, the ideal gas equation of state, the induction equation for the magnetic field, and Ampére's law, neglecting the displacement current:

$$\frac{\partial \rho}{\partial t} + \nabla \cdot (\rho \mathbf{v}) = 0\,, \tag{2.3}$$

$$\rho \frac{d\mathbf{v}}{dt} = -\nabla P + \rho g \hat{\mathbf{z}} + \frac{1}{c_l} \mathbf{J} \times \mathbf{B}\,, \tag{2.4}$$

$$C_v \rho \frac{dT}{dt} + P \nabla \cdot \mathbf{v} = Q(T, \rho)\,, \tag{2.5}$$

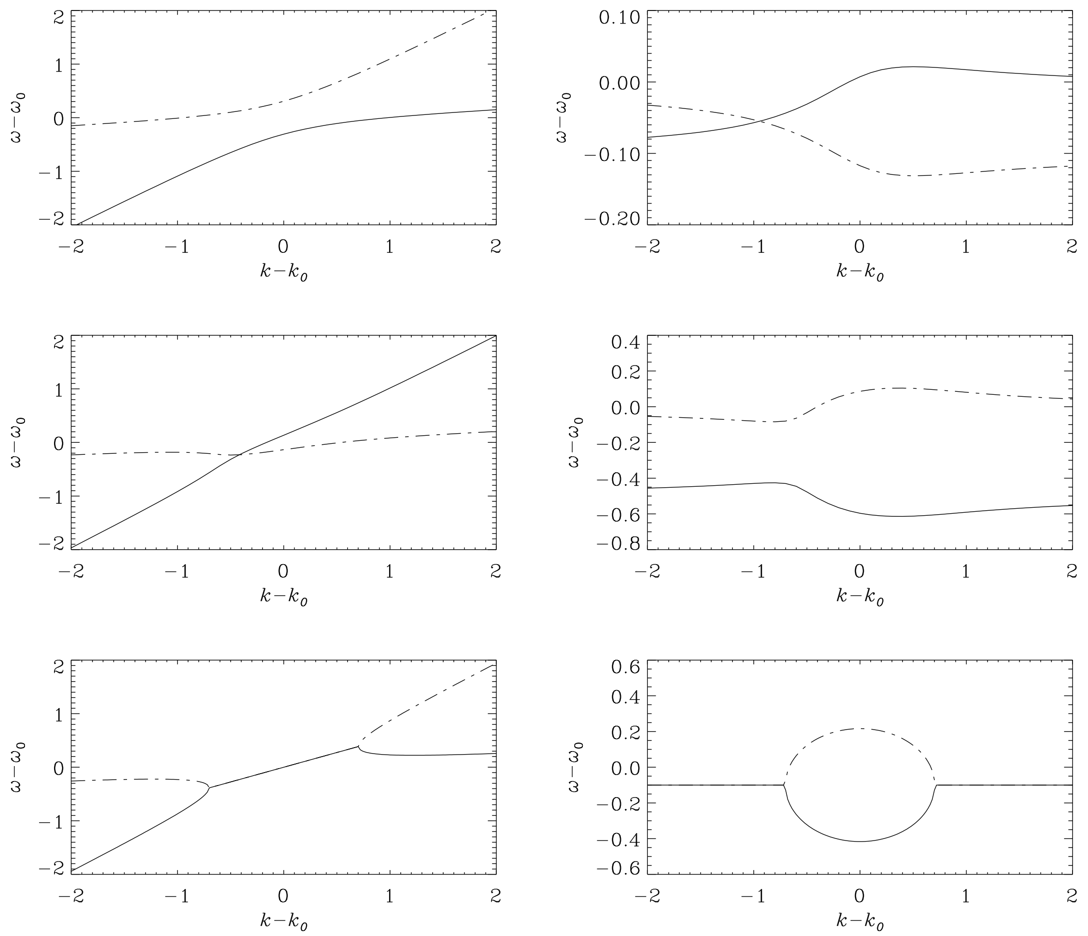

Figure 2.1: Three sets of solutions of the (complex) quadratic: $[\omega - \omega_0 + \alpha i - u(k - k_0)]\,[\omega - \omega_0 + \beta i - v(k - k_0)] - \epsilon = 0$. We fix $u = 1.0$ and $v = 0.1$ and vary α, β and ϵ. We show each set as the real and imaginary parts of $\omega - \omega_0 = F(k - k_0)$. Top panel: $\alpha = 0.1$, $\beta = 0.01$ and $\epsilon = exp(-\pi i/8)$; middle panel: $\alpha = 0.01$, $\beta = 0.5$ and $\epsilon = exp(5\pi i/8)$; bottom panel: $\alpha = 0.1$, $\beta = 0.1$ and $\epsilon = -1$.

$$P = R\rho T\,, \tag{2.6}$$

$$\frac{\partial \mathbf{B}}{\partial t} = \nabla \times (\mathbf{v} \times \mathbf{B})\,, \tag{2.7}$$

$$\mathbf{J} = \frac{c_1}{4\pi}\nabla \times \mathbf{B}\,, \tag{2.8}$$

and R and C_v are the gas constant and heat capacity (at constant volume) of our ideal gas. The gravitational acceleration is $g\hat{\mathbf{z}}$ and z is the vertical spatial coordinate, taken to be increasing downwards. The heat loss function Q we take to be given by Newton's law of cooling (e.g. Spiegel, 1957).

In hydrostatic equilibrium there is no flow and the state variables depend only on z. There is no current in the background state ($\boldsymbol{\nabla} \times \mathbf{B}_0 = 0$) so the background magnetic field does not alter the background pressure and density profiles.

For an isothermal slab, the pressure and density depend exponentially on depth with a scale height $H = RT_0/g$. The sound speed is constant and the Alfvén speed, $B_0/\sqrt{4\pi\rho_0}$, decreases exponentially with depth. In the case of interest here, the background temperature profile is assumed to increase linearly with depth, $T_0 = \beta z$. Then the density is of the form $\rho_0 = \rho_*(\frac{z}{z_*})^m$ with $m = \frac{g}{R\beta} - 1$ and the pressure has the form $P_0 = P_*(\frac{z}{z_*})^{m+1}$, with ρ_*, P_*, and z_* as the characteristic density, pressure, and length scales. The pressure and density are related polytropically, $P_0 \propto \rho_0^{\frac{m+1}{m}}$, though for slightly different reasons than for conventional polytropes. To facilitate computations, we have chosen to confine the layer under study between two positive values of z.

2.4 Linear Theory

The linearized equations are separable in time and in the horizontal and vertical coordinates. Therefore, we may seek linear solutions in the form $f(z)\exp[i(kx - \Omega t)]$ where x is the horizontal coordinate.

For Newton's law of cooling (Spiegel, 1957) we have

$$Q = -q\rho C_v \Theta \tag{2.9}$$

where q is the inverse of the characteristic cooling time and Θ is the temperature perturbation. Newton's law of cooling is correct to first order for perturbations to homogeneous optically thin backgrounds (Osaki, 1966); this result can easily be extended, in the case of constant opacity coefficient, to the optically thin stratified case. In general though the cooling function Q depends on both the density and temperature perturbations (e.g. Field, 1965). The application of Newton's law of cooling to generic stratified media is, however, standard in the literature (e.g. Syrovat-skii & Zhugzhda, 1968; Souffrin, 1972; Mihalas & Toomre, 1982; Hasan, 1986; Umurhan et al., 1999). Christensen-Dalsgaard & Frandsen (1983) discuss the radiative transfer problem for solar oscillations in some detail.

In this work we consider only the case of constant inverse cooling time q. In the chromosphere, however, the cooling time ranges over a few orders of magnitude (Gibson, 1973); a detailed modeling effort should certainly take this into account. In this work we are only attempting to find qualitative patterns. We are not in any way attempting to build a realistic model chromosphere.

With Newton's law of cooling the linearized equations read:

$$\rho' = \frac{q - i\Omega}{q - i\gamma\Omega} P' + \frac{1}{q - i\gamma\Omega}\left(\frac{d\log P_0}{dz} - \gamma\frac{d\log\rho_0}{dz}\right)W' \,, \tag{2.10}$$

$$-i\Omega\rho' + \frac{d\log\rho_0}{dz}W' + ikU' + \frac{dW'}{dz} = 0 \,, \tag{2.11}$$

$$\Omega U' = \frac{kc^2}{\gamma}P' - \frac{a^2}{\Omega}\left(\frac{d^2U'}{dz^2} - k^2U'\right), \tag{2.12}$$

$$-i\Omega W' = -\frac{c^2}{\gamma}\left(\frac{dP'}{dz} + \frac{d\log P_0}{dz}P'\right) + g\rho' \,, \tag{2.13}$$

$$a^2 = \frac{{B_0}^2}{4\pi\rho_0} \quad , \quad c^2 = \frac{\gamma P_0}{\rho_0} \,. \tag{2.14}$$

Here P' and ρ' are the ratios of the pressure and density perturbations to their background values; U' and W' are the horizontal and vertical components of the velocity; a and c are the Alfvén and sound speeds, which in general are functions of depth; and γ is the ratio of specific heat at constant pressure to specific heat at constant volume.

We take $W' = 0$ and $\frac{dU'}{dz} = 0$ as our velocity boundary conditions on the top and bottom of the layer. These boundary conditions were chosen to eliminate the flux of mechanical and magnetic energy through the boundaries (see Appendix A). The resulting two-point boundary-value eigenvalue problem is then *self-adjoint* for the isentropic ($q = 0$) case, which has been studied by Bogdan & Cally (1997) for a semi-infinite atmosphere.

2.5 Numerical Results

Like previous workers, we find complicated patterns of avoided crossings and mode mergers when we examine the $k - \Omega$ diagrams for various parameters. We focus, however, only on the weak magnetic field case for the purposes of this discussion. For all of the numerical results presented here, the ratio of Alfvén speed to sound speed at the bottom of the layer is 0.1, $\gamma = 5/3$, and the layer extends across 4.6 density scale heights.

We present the results as functions of the dimensionless horizontal wavenumber kD, where k is the horizontal wavenumber and D is the layer thickness. The time constant is $\Omega = \omega + i\eta$ where the frequency ω and the growth rate η are real and are presented in dimensionless form as $\omega\tau$ and $\eta\tau$ where $\tau = D/c_b$ and c_b is the sound speed at the bottom of the layer. Whenever comparison is made between polytropic and isothermal atmospheres, it is always made between layers with the same γ, the same number of density scale heights, and the same ratio of Alfvén speed to sound speed at the bottom of the layer.

2.6 Large Cooling Time

A typical $k - \omega$ diagram for a weakly magnetized polytrope with small q is shown in Figure 2.2. Figure 2.3 exhibits the corresponding growth rates, in addition to frequencies, for the first four branches of the polytropic and isothermal atmospheres. The modes can be clearly identified at small and large k. In between, there is a series of avoided crossings and mode classification becomes ambiguous.

For $k = 0$ the modes can be identified as either incompressible transverse Alfvén waves or longitudinal acoustic oscillations, unaffected by the magnetic field. Notice that the Alfvén mode with $k = 0$, vertical wavenumber zero, and frequency

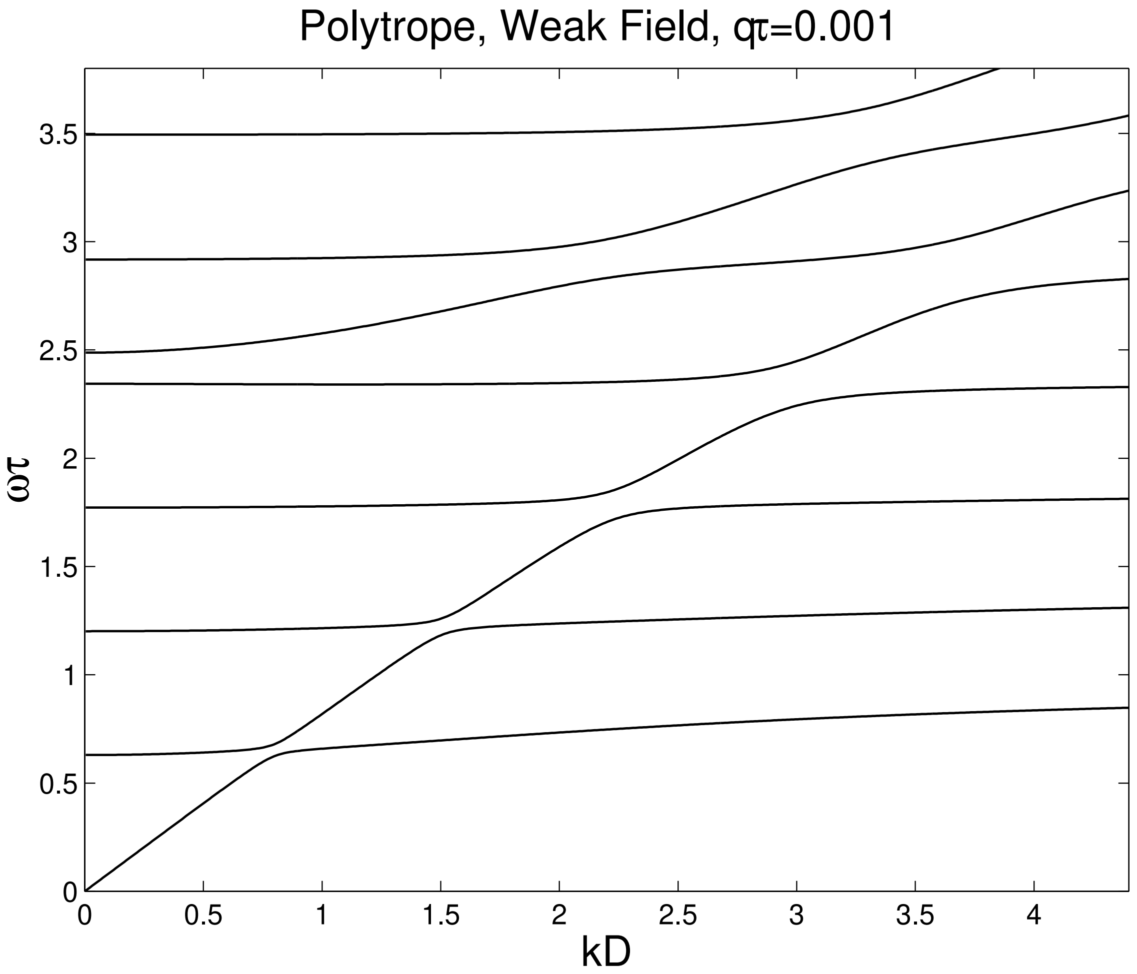

Figure 2.2: Frequency as a function of horizontal wavenumber k for the first eight modes of an $m = 2$ polytrope atmosphere with weak magnetic field and weak damping, $q\tau = 10^{-3}$. The ratio of Alfvén speed to sound speed is 0.1 at the bottom of the layer. The layer extends over 4.6 density scale heights. We note that every mode shown along $k = 0$, except the sixth, is an Alfvén mode.

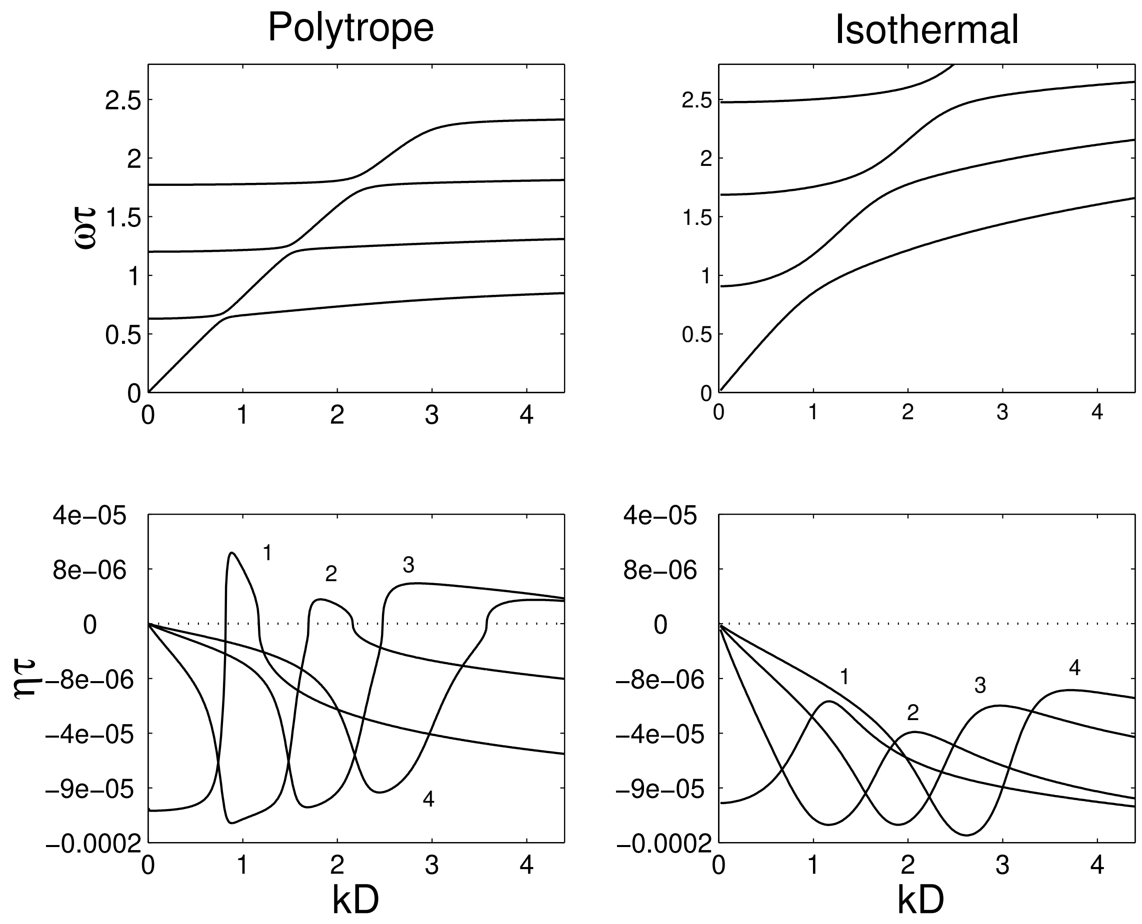

Figure 2.3: The frequencies, in the upper two plots, and growth rates, in the lower two plots, as functions of horizontal wavenumber k for the first four branches of both an $m = 2$ polytrope, shown on the left, and isothermal, shown on the right, atmosphere with weak magnetic field and weak damping, $q\tau = 10^{-3}$. The ratio of Alfvén speed to sound speed is 0.1 at the bottom of both layers and both layers extend over 4.6 density scale heights. The branches are labeled in the lower plots in order of increasing frequency. For the polytrope, the first four branches are overstable for small ranges in k. For the isothermal atmosphere, all of the modes are damped. Note the scale on the $\eta\tau$ axis is not linear; this is done to make the main features more visible.

zero, is allowed by our boundary conditions. This corresponds to a global, volume-preserving motion that would be excluded by physically motivated boundary conditions.

As k increases from zero, the acoustic modes increase in frequency, just as with p-modes in the absence of magnetic field. The magnetic modes (m-modes) remain approximately transverse as k increases from zero; as a result, the modes remain essentially pure transverse Alfvén modes with frequencies dependent only on their vertical wavenumbers. For small k, the displacement of such a mode is mainly horizontal and thus the frequency is unaffected, to lowest order in k, by the buoyancy force. The Alfvén mode with zero frequency becomes the magnetically-modified Lamb mode with increasing k.

For large k, the modes are either the fast or slow MHD modes. The fast mode that propagates across the background magnetic field is the magnetosonic mode, which is longitudinal and has the gas and magnetic pressures as restoring forces. For large k, its frequency is proportional to k. The slow mode propagating almost across the background field has mainly magnetic tension and buoyancy as restoring forces and, as k increases, the frequency goes to a constant set by the vertical wavenumber, the Alfvén speed, and the buoyancy frequency.

For intermediate values of k the character of the modes is mixed and classification is difficult. The generic pattern is of avoided crossings and mode mergers. As k increases the frequencies of the p-modes and the frequency of the Lamb mode both increase while the frequencies of the m-modes are approximately constant. Thus, crossings of different modes are inevitable and mode interaction is clearly present.

The growth rates in Figure 2.3 show many sharp features. The first four branches in the polytropic atmosphere are unstable in some ranges of horizontal wavenumber. The instability appears when the branch approaches an avoided crossing from below. Near avoided crossings the character of the modes becomes mixed.

A comparison of growth rates with those for the isothermal atmosphere, in Figure 2.3, reveals that the basic pattern is the same for both cases. The growth rate is maximum as the branch approaches an avoided crossing from below.

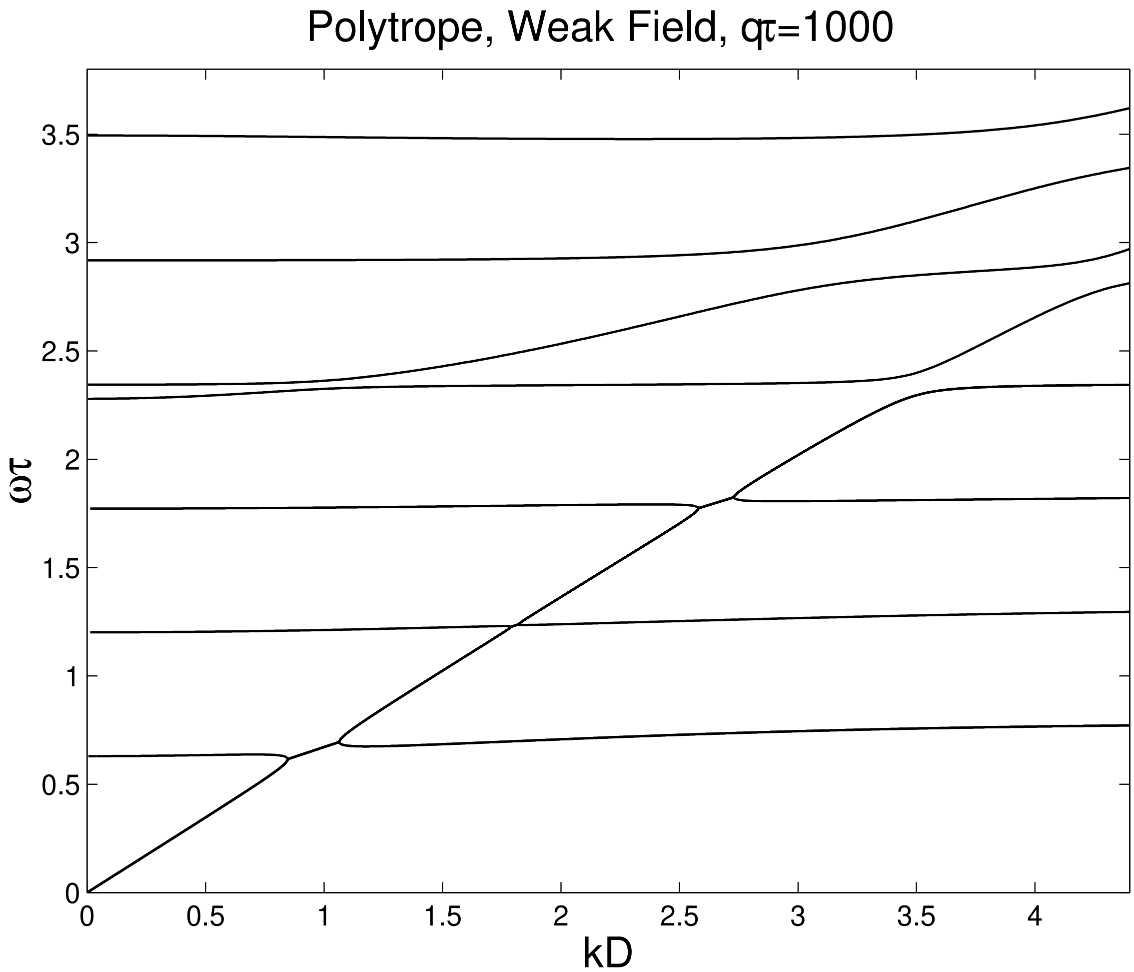

Figure 2.4: The frequency as a function of horizontal wavenumber for the first eight branches in the polytropic atmosphere with $m = 2$. The ratio of Alfvén speed to sound speed is 0.1 at the bottom of the layer and the layer covers 4.6 density scale heights. The dimensionless inverse cooling time $q\tau$ is 10^3. Notice that instead of avoided crossings, as are present in the low q case, there are now mergers of the frequencies for the low order modes. The mode mergers are seen only for small ω. For large ω, avoided crossings are seen as in the small q case.

2.7 Small Cooling Time

New behavior is seen for large q. A typical diagnostic diagram is shown in Figure 2.4. Instead of the avoided crossings seen at small q we now see mergers in the $k - \omega$ diagram. The left panels of Figure 2.5 show growth rates, as well as frequencies, for the case shown in Figure 2.4. The right panels of Figure 2.5 show the first two branches of the corresponding isothermal atmosphere, for purposes of comparison.

For the polytropic case the growth rates, for low order modes, show large features where two branches merge in frequency. In the limit of infinite q, where the temperature perturbation is asymptotically zero, these features remain. Then we can show that the two (complex) frequencies are complex conjugates at the merger so that the presence of one damped mode implies the presence of a growing mode.

As seen in Figure 2.5, the growth rates in the isothermal and polytropic cases are not unrelated. Where the first growing/decaying pair appears in the polytrope, we see a corresponding peak and valley in the growth rates along the first and second branches of the isothermal case.

2.8 A Resonant Hopf Bifurcation

We have performed a systematic stability analysis of oscillations in non-adiabatic, stratified magnetized atmospheres. Rather than reporting further details, we simply indicate the presence of resonant Hopf bifurcations, which should simplify the continuation of this work into the nonlinear regime.

To illustrate, let us consider the avoided crossings in a sequence of model atmospheres. In Figure 2.6, we show the crossing of the first and second modes in atmospheres with increasing values of q. At low q, the usual avoided crossing is seen (top panel). As q is increased, the distance between branches at the avoided crossing becomes smaller until the frequencies cross and the avoidance appears instead in the growth rates (middle panel). As q is increased even more, at a critical value, the frequencies merge and features appear in the growth rates where the real parts of the frequencies are equal (bottom panel).

Quite a few tell-tale characteristics of the avoided crossings are reproduced by simple dispersion relations of the form (eq. [2.2]) with damping independent of k

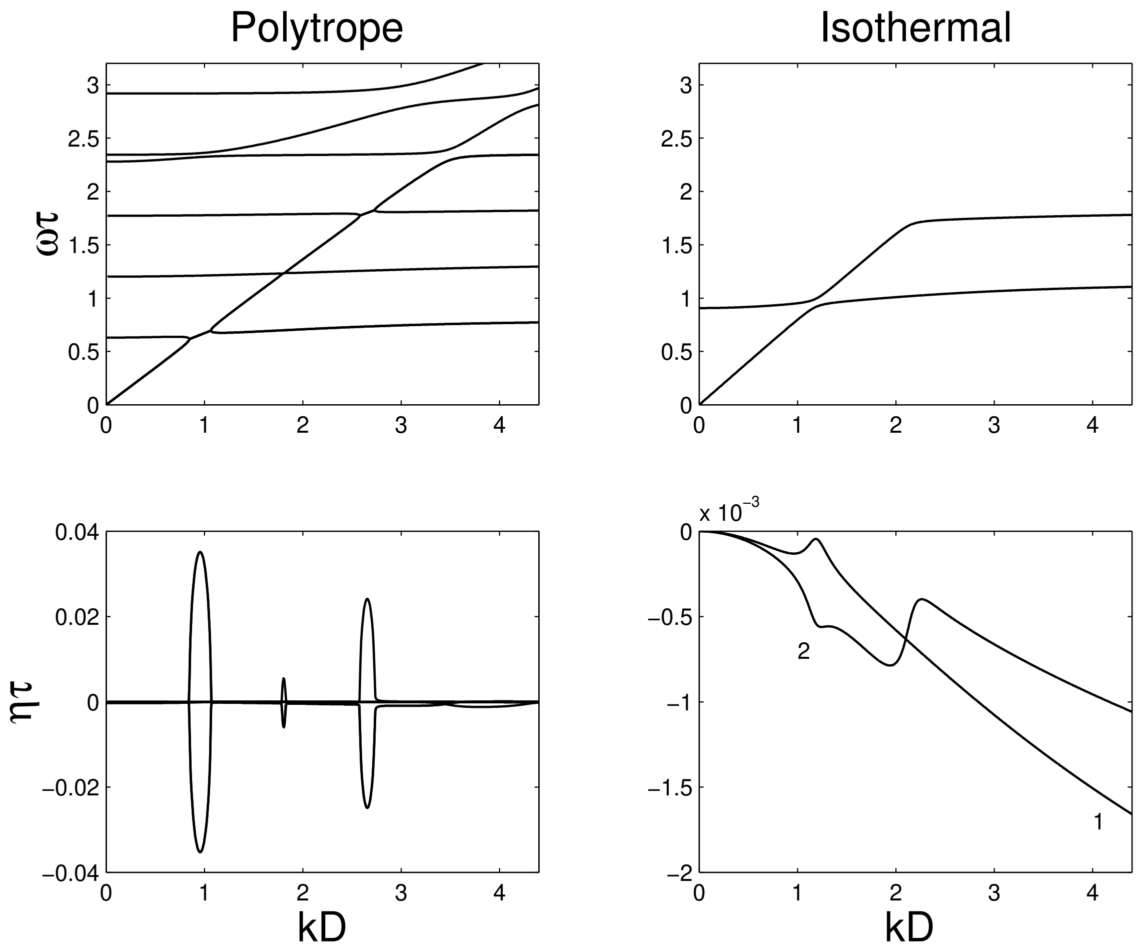

Figure 2.5: The frequencies, in the top panels, and growth rates, in the lower panels, are shown for polytrope, on the left, and isothermal, on the right, layers. The polytrope layer is the same as in Figure 2.4. Both the isothermal and polytropic layers have $q\tau = 10^3$, cover 4.6 density scale heights, and have a ratio of Alfvén speed to sound speed of 0.1 at the bottom. For clarity, only the first two branches are shown for the isothermal atmosphere. Where mergers in frequency occur there are large features in the growth rates, many orders of magnitude larger than for the low q case. For the polytrope, when the real parts of the frequencies merge, the two branches at the merger become complex conjugate pairs; one mode is growing and the other decaying. Notice that where the polytrope atmosphere shows a merger, there is an avoided crossing in the diagram for the isothermal atmosphere, accompanied by features in the growth rate.

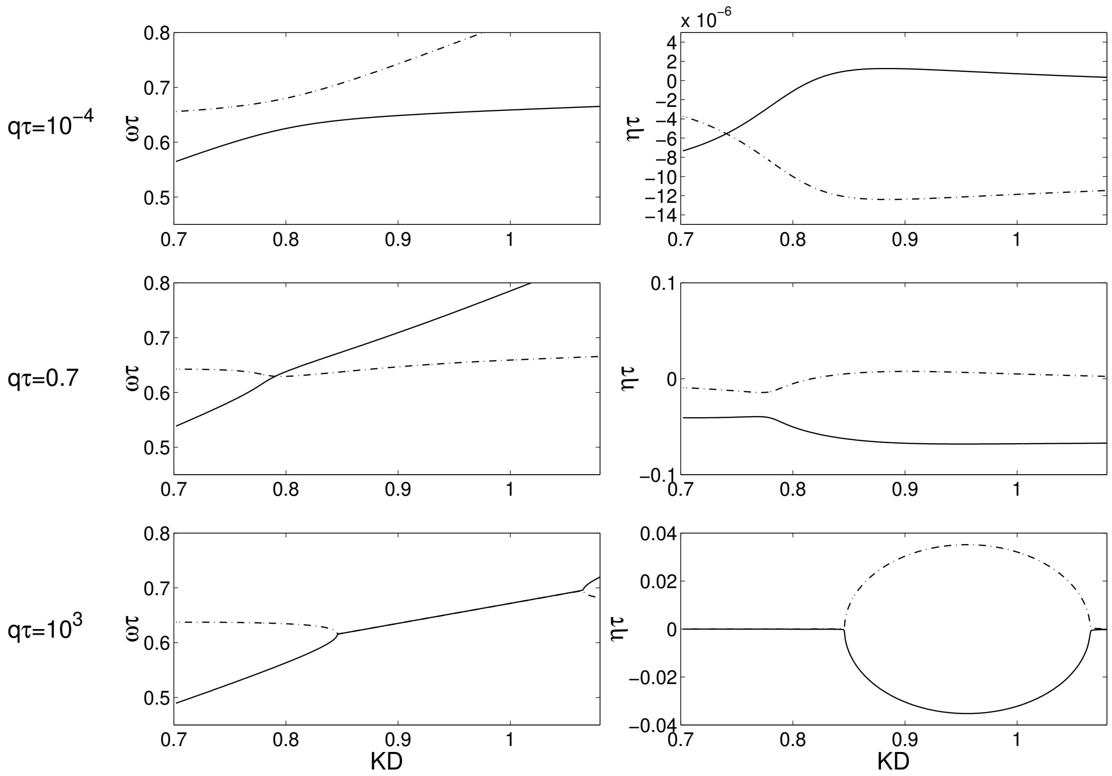

Figure 2.6: Frequency, on the left, and growth rate, on the right, are shown as functions of kD for the first two branches of the $m = 2$ polytrope with 4.6 density scale heights and magnetic Mach number (a/c) of 0.1 at the bottom of the layer. Only the vicinity of the crossing is shown. The three pairs of plots are for three different values of the cooling time, $q\tau = 10^{-4}, 0.7$, and 10^3. The plots proceed from small q on the top to large q on the bottom. The first branch is shown in the solid line and the second branch in the dashed line. As q increases the transition from avoided crossing to merger is seen. Notice that the vertical scales on the plots of the growth rates are different; this is done to show detail. Note the similarity between this figure and Figure 2.1.

at resonance. In the weak q case, the crossing of the damping rates occurs for a k smaller than the horizontal wavenumber at resonance, while the maximum growth and damping rates occur at a larger k. For intermediate q, the distinctive bumps at the crossing of the frequencies are also captured by our simple model (compare the middle panels of Figure 2.1 and 2.6).

This sequence is generic to our numerical results and, if we may judge from the astrophysical literature, to stellar atmospheres in general. This range of behavior can be explained by the onset of resonant oscillatory bifurcations, as in Figure 2.1, and it forecasts the occurrence of overstability and strong damping near avoided crossings, as reported by previous workers (Banerjee et al., 1997; Gore, 1997). In each of the three cases, the imaginary part of the frequency increases or decreases away from the crossing, leading to strong mode quenching or amplification near the crossing. Therefore, the primary role of non-adiabaticity is to set the reference level for the growth or decay rates at crossings.

For the Sun the cooling rate, q, depends on radius. In the chromosphere the cooling time is very roughly of order 300 s, it varies by about two orders of magnitude over the height of the chromosphere (Gibson, 1973) . The sound speed crossing time, τ, is also roughly 300 s, so that the dimensionless cooling rate $q\tau$ is approximately of order unity. Thus the chromosphere is intermediate between the large and small $q\tau$ cases that we have presented in detail here.

2.9 Islands of Reality: the Onset of Complex Eigenvalues

So far, we have discussed only *local* properties of resonant Hopf bifurcations. We have seen that the simplest model of two resonant, damped modes in equation (2.2) adequately describes the range of behavior seen near avoided crossings where oscillations may become linearly unstable. This indicates that the instability is intimately linked with the complexity of the coupling ϵ, but what is responsible for the instabilities?

If we study the acoustic oscillations of an atmosphere in terms of a two-point boundary-value eigenvalue problem, we find that, in the adiabatic case, with suitable boundary conditions, the relevant linear operators are self-adjoint. This ensures that the eigenvalues (here the squares of the frequencies) are real. The appearance of overstable modes, or complex eigenvalues, is associated with the loss of the *self-adjoint* property that we normally attribute to non-adiabatic effects — thermal conduction or viscous effects — and this appears to be generic (Umurhan, 1999). Thermal and viscous losses lead to complex coupling between resonant modes. Even in the presence of ideal conditions, however, with certain boundary conditions the relevant operators, as in equations (2.10)-(2.13), can become non-self adjoint, as many examples have revealed.

In the field of non-radial adiabatic oscillations in rotating stars, Lee & Saio (1990) found overstability in their dispersion relation. In a study of magnetic oscillations of isothermal atmospheres, Banerjee et al. (1995) pointed out the disappearance of purely real frequencies when they applied certain sets of boundary conditions for the boundary-value eigenvalue problem. They reported localized islands in the frequency versus horizontal wavenumber plots. That is to say, for particular branches of magnetoacoustic oscillations, there are ranges in the horizontal wavenumber where the frequency is complex, signalling either evanescence or instability. Banerjee et al. (1995) regarded the solutions with complex frequency as unrealistic and plotted only the real frequencies. This raises the question, however, of what non-self adjointness and complex frequencies imply for the waves within particular ranges of horizontal wavenumbers. This issue arises in other fluid flow problems and notably in plasma physics, where it becomes a question of *absolute* versus *drift* instability.

In our atmospheric model, an oscillatory disturbance can evolve in two different ways. The wave can grow or decay in place; this is the usual picture for unstable or stable oscillations. In certain cases, the wave can grow and propagate away from the origin of the disturbance. For an infinite medium in this latter regime, at a fixed point in space, the disturbance decays with time, though the wave may be growing away from the point of disturbance. This is the situation with vertically propagating acoustic waves in an isothermal atmosphere.

These two distinct physical situations, corresponding to *absolute* and *drift* (or *convective*) instabilities, are understood in a infinite medium. In a finite atmosphere such as in our model, the evolution of a wave suffering from drift instability depends on the boundary conditions and their influence on the self-adjointness of the linear operator. We defer this technical issue to Appendix A.

2.10 Discussion

Nonadiabatic acoustic perturbations to atmospheres with temperature stratification are subject to instabilities for a variety of reasons, not all of which have been clarified physically. Nevertheless several investigations have shown that these instabilities are common in thin layers of stars, such as the solar chromosphere. For such layers, much wider than they are deep, the spectrum of the frequencies of the unstable modes, as functions of horizontal wavenumber, will be dense and may be treated as *continuous*. This is a situation in which the evolution of the envelope of the modal amplitudes may be expected to satisfy the complex Ginzburg-Landau equation (e.g. Manneville, 1990), a partial differential equation in horizontal coordinates and time. Under suitable conditions, this equation produces spatially localized oscillatory structures (Umurhan et al., 1999) like the oscillons seen in shaken granular media (Umbanhowar et al., 1996).

The generation of localized structures from the nonlinear development of a continuous band of overstable modes is of interest in the present context because it is often thought that some special mechanism, perhaps related to magnetic fields, is needed to produce sharply defined structures like solar spicules. This is not the case, as we see from the example just described. Nevertheless, the recent discovery of the magnetic carpet (Title & Schrijver, 1998) at a suitable height in the solar atmosphere makes it clear that the involvement of magnetic fields in the formation of spicules can hardly be doubted. It is known that overstabilities of stratified nonadiabatic media are also present when magnetic fields are introduced (Syrovatskii & Zhugzhda, 1968; Christensen-Dalsgaard, 1981; Babaev et al., 1995; Gore, 1997). But while we believe that solar magnetic fields are significant in shaping spicules, we do not regard it as necessary to assume that the fields play a causative role in spicule formation. Rather our interest in the magnetic fields is motivated by their promotion of *resonant* oscillatory instabilities as signaled by the avoided crossings recalled here.

The nonlinear amplitude equations for the resonant Hopf bifurcation are readily written down using techniques that have been discussed in many places for the case of *discrete* modes (Guckenheimer & Holmes, 1983; Elphick et al., 1987) and some preliminary studies have been described (Buchler et al., 1997). In the case of a situation like the chromosphere, we need the generalization to the case of pattern equations (equations describing the development of the amplitudes of a continuum of modes). As far as we are aware, the relevant equations for this case have not been exhibited, let alone studied. Yet the present work suggests, if rather abstractly, that such equations would have much to teach us. The Ginzburg-Landau equation is the relevant pattern equation for a single overstable mode. With a resonant pair of such modes we would anticipate a coupled set of Ginzburg-Landau equations. These would be capable of producing negative energy solutions, which lead to a phenomenon known as explosive behavior. The results reported here indicate that this could be of interest for studies of chromospheric fluid dynamics.

This work began when three of us (ACB, EAS, and LT) were participants in the Geophysical Fluid Dynamics Summer Program at the Woods Hole Oceanographic Institution in 1998. J. Biello was particularly helpful during that period. During the preparation of the manuscript we benefited from discussions with J. Christensen-Dalsgaard, P. Cvitanović, P. Pechukas, and O. M. Umurhan.